QUASI-IDEALIZED SIMULATIONS OF BOW ECHOES

Nolan T. Atkins*
Lyndon State College, Lyndonville, Vermont

1. INTRODUCTION

Bow echoes are a well-known mode of severe convection that often produce long, narrow swaths of straight-line wind damage and tornadoes. Fujita (1978) was the first to hypothesize that downburst winds in a descending rear-inflow jet (RIJ) were responsible for generating the observed straight-line wind damage swaths at the apex of the developing bow echo. It was also noted that the tornado damage was often found at or north of the bow apex.

Recent observational (e.g., Atkins et al. 2005) and modeling studies (e.g., Trapp and Weisman 2003) have discussed how small scale, (1-10 km) low level (0-5 km AGL) "mesovortices" formed on the leading of bow echoes may also play a role in generating wind damage within bow echoes. As summarized in Fig. 1, Atkins et al. (2005) have shown that mesovortices can produce long narrow swaths of straight-line wind damage north of the bow apex. The mesovortices were also responsible for producing F0-F1 tornadoes.

The idealized modeling study by Trapp and Weisman (2003) showed that the mesovortices are produced by precipitation-loaded downdrafts tilting baroclinically-generated horizontal vorticity into vertical vortex pairs. Convergence of planetary vorticity enhances the cyclonic member with time. The generality of this mesovortex genesis mechanism is not well known.

The objective of this study is to use WRF to simulate the bow echo event discussed by Atkins et al. (2005) where mesovortices produced straight-line wind and tornado damage. The emphasis of this work is to understand the generation mechanism(s) of the mesovortices and what factors control vortex strength.

2. WRF MODEL INITIALIZATION

The bow echo event of interest occurred on the afternoon of 10 June 2003 over the greater Saint Louis, MO area. A sounding launched at 18 UTC at Springfield, MO was used to initialize WRF. The sounding data indicated that the air mass initiating the convective system contained about 2560 J kg^{-1} of CAPE and moderate low-level wind shear. Convection was initiated in the model by introducing three thermal bubbles oriented north-south spaced 40 km apart in the center of the domain. The domain was 400 x 400 km in the horizontal direction with a grid spacing of 1 km. The vertical grid spacing varied from 110 m near the ground to just over 1 km at

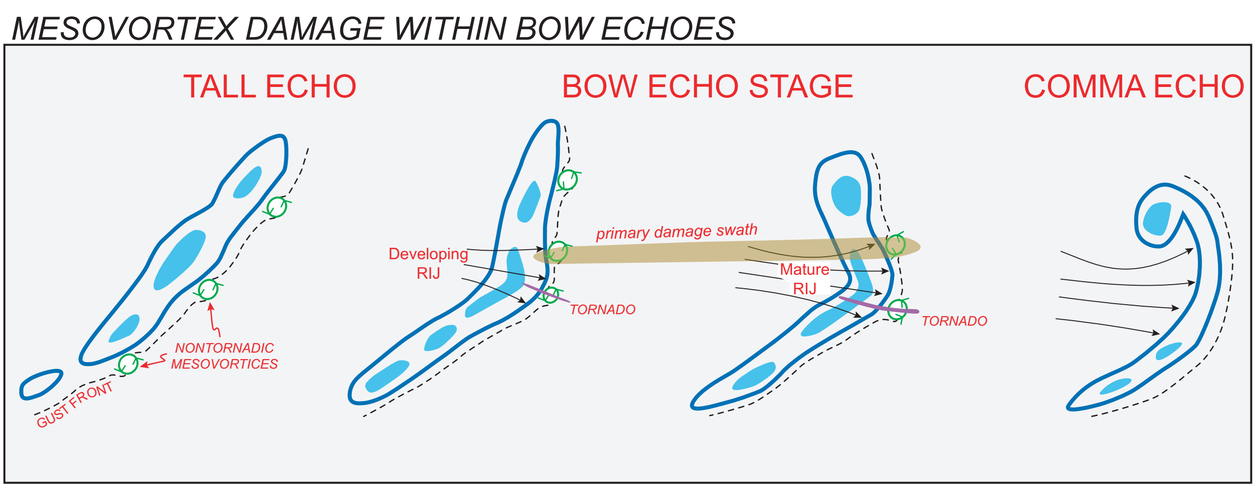

Figure 1. Schematic diagram of wind damage produced within bow echoes based on radar and damage survey analysis of the 10 June 2003 St. Louis bow echo event during the Bow Echo and MCV Experiment (BAMEX). Radar reflectivity is contoured and filled in blue. Mesovortex locations are indicated in green. Tornado damage in indicated in purple while staight-line wind damage is shown in brown.

**Corresponding Author Address*: Dr. Nolan T. Atkins, Department of Meteorology, Lyndon State College, Lyndonville, VT 05851; email: nolan.atkins@lyndonstate.edu

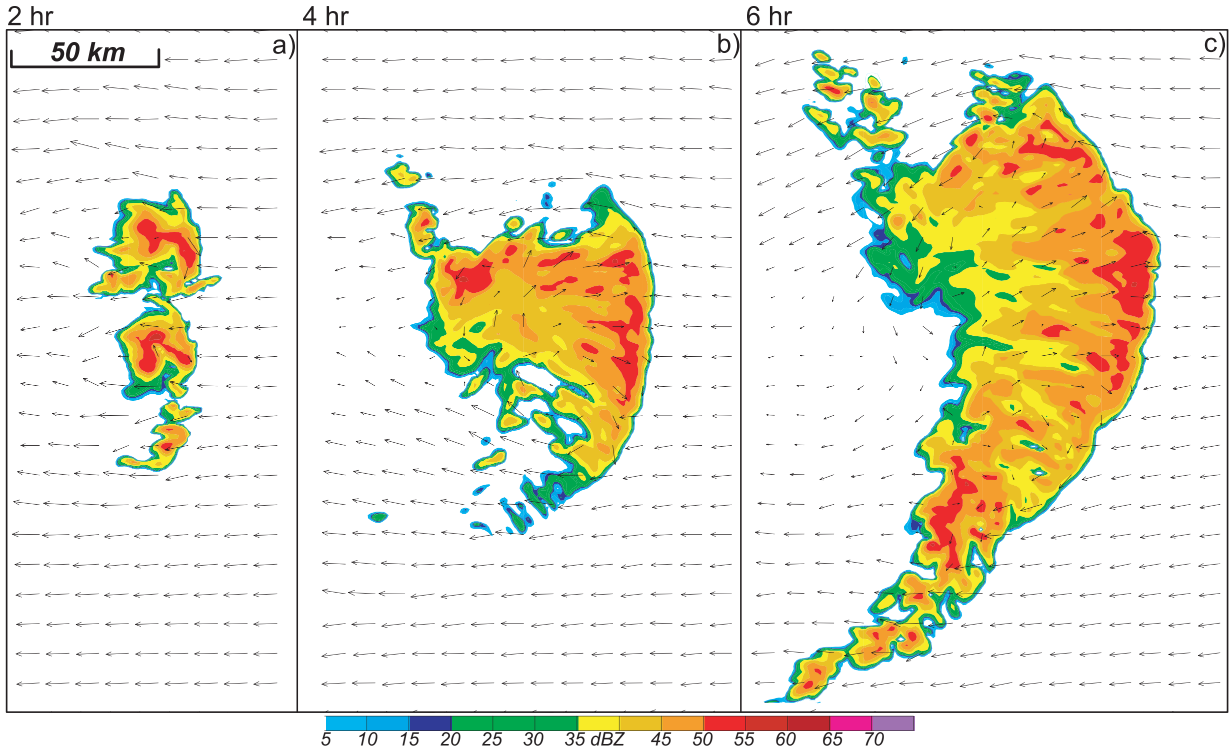

Figure 2. Simulated radar reflectivity (color) at 0.15 km AGL and horizontal storm-relative winds (black vectors) at 1.3 km AGL at a) 2 hours, b) 4 hours, and c) 6 hours into the simulation. Storm motion of 22 and 6 ms^{-1} in the west-east and south-north directions, respectively was removed from the ground relative wind field.

the top of the domain located 17250 m AGL. The lateral boundaries were open while the surface was free slip. The simulations were run using the Lin ice microphysics scheme available in WRF. The coriolis force was allowed to act only on the perturbations of the flow. Turbulence was parameterized with the 1.5 order TKE closure scheme.

3. OVERVIEW OF CONTROL RUN

The evolution of the simulated bow echo is shown in Fig. 2 where the simulated radar reflectivity field at 0.15 km above ground level (AGL) and storm-relative winds at 1.3 km AGL are plotted at 2, 4, and 6 hours. At 2 hours, three storms initiated by the initial thermal bubbles are evident. Two hours later, an organized line of bowing cells had developed. The wind field at 4 hours clearly showed the presence of a pair of line-end vortices and RIJ between them. By 6 hours (Fig. 4c), the bow echo had evolved into an asymmetric structure with a large prominent cyclonic circulation at the northern end of the convective line. The RIJ and intense line of bowing convective cells were again evident. The system had grown in spatial scale from 2 to 6 hours. The scale, orientation, and structure of the simulated bow echo at 6 hrs (Fig. 4c) was qualitatively similar to the observed bow echo documented by Atkins et al. (2005) (not shown).

A more detailed examination of the bow echo at 5.5 hours into the simulation is shown in Fig. 3. The presence of low-level circulations was clearly seen in Fig. 3a along the leading edge of the bow echo. Two prominent cyclonic mesovortices (labeled #1 and #2) were observed, collocated with appendages in the radar reflectivity field. An even more detailed depiction of mesovortex #2 is shown in Fig. 3b. This vortex exhibited a closed circulation in the wind field with a vertical vorticity magnitude of about 20 x 10 $^{-3}$ s^{-1}. The vortex position was again seen to be collocated with an appendage of the radar reflectivity field. It was also observed to be on the cool-air side of the gust front. These results are similar to the structure and position of the idealized mesovortices discussed by Trapp and Weisman (2003).

The vertical structure of mesovortex #2 is shown in the vertical cross section in Fig. 4. The cross section location is shown as the black line oriented southwest to northeast in Fig. 3c. This cross section orientation was chosen since it represents the direction that the vortex tilted along the gust front.

The tilt of the mesovortex is clearly seen in Fig. 4. The mesovortex was located just behind the gust front in

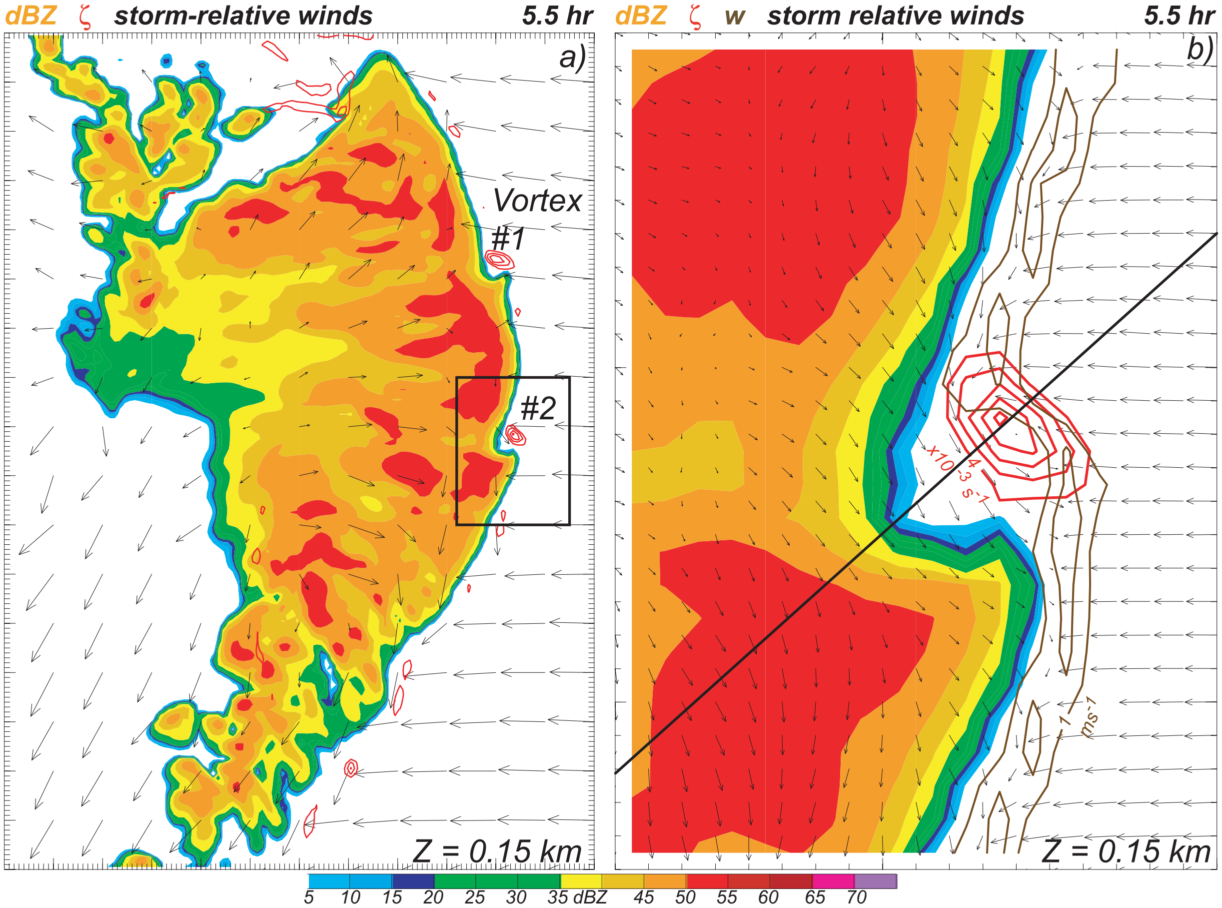

Figure 3. a) Simulated radar reflectivity (dBZ; color), vertical vorticity (x 10^{-3} s^{-1}; red), and storm-relative winds (ms^{-1}; black vectors) are all plotted at 0.15 km AGL. Vertical vorticity is contoured beginning at 4 x 10^{-3} s^{-1}, every 4 x 10^{-3} s^{-1}. The black box is the area shown in b). b) All fields are the same as in a) except vertical velocity is also contoured in brown beginning at 1 ms^{-1}, every 1 ms^{-1}. The black line in b) is the location of the vertical cross section shown in Fig. 4.

the cool air and tilted rearward along the gust front. The mesovortex appeared to extend at least to 5 km AGL. The larger vertical vorticity values of at least 16 x 10^{-3} s^{-1} were located near the ground. The vortex was also embedded in updraft suggesting that stretching may play a role in the amplification of the mesovortex with time.

4. SENSITIVITY STUDIES

A number of sensitivity experiments were performed to examine the impact of ice microphysics, the coriolis parameter, and surface drag on the structural evolution of the system and sub-system scale features observed in the control run presented in section 3. A brief description of the sensitivity experiments is presented herein, more detailed results will be shown at the workshop.

It has been shown that varying the size distribution of hail within the Lin ice microphysics scheme noticeably affects the strength of supercell cold pools. A series of experiments were, therefore run to see if a similar result could be observed with bow echoes. With hail size distributions where more mass was shifted into the larger sizes, the bow echo cold pool was spatially smaller and weaker. In fact, by shifting enough mass into the larger hail sizes, it was possible to weaken the cold pool to the point where a long-lived convective system was not produced. Thus, the structural evolution of simulated bow echoes appears to be very sensitive to the size distribution of hail within the Lin ice microphysics scheme.

When the coriolis parameter was turned off, a well-defined bow echo was formed and had a similar structure as observed in the control run for the first 3 hours. Thereafter, as might be expected, the bow echo not subjected to the coriolis force evolved differently. A significant difference between the control and no coriolis runs concerned the mesovortices. Significant anticyclonic mesovortices were observed along the leading edge of the bow echo only when the coriolis force was turned off

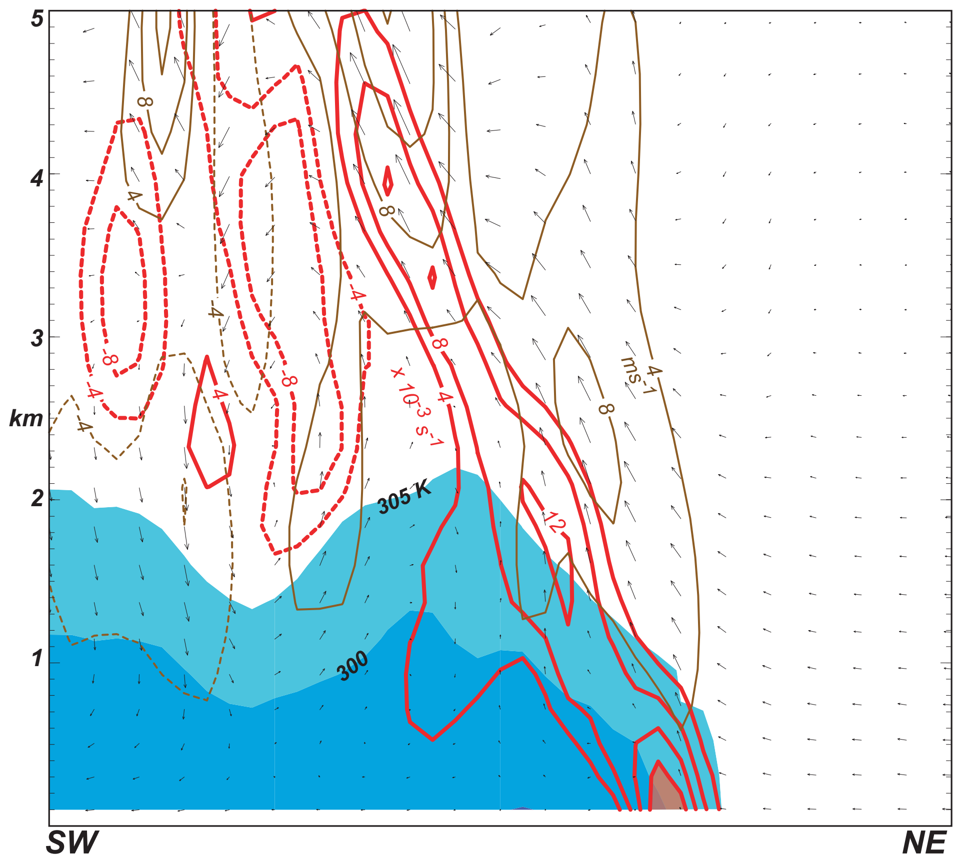

Figure 4. Vertical cross section of potential temperature (K; color-filled blue), vertical velocity (ms^{-1}; brown), vertical vorticity (x10^{-3} s^{-1}; red), and storm-relative winds in the plane of the cross section (ms^{-1}; black arrows). The cross section location is shown as the black line in Fig. 3b.

in the model. This result suggests that the coriolis parameter may be important for the evolution of mesovortices.

5. CONCLUSIONS

A quasi-idealized simulation of an observed bow echo on 10 June 2003 has been presented. Similar to the observed bow echo, the control simulation produced a bow echo that had qualitatively similar system-scale features, including book-end vortices, RIJ, and intense line of bowing cells. The simulation also contained small-scale "mesovortices" formed on the leading edge of the bow echo. Their structure was shown to be consistent with observational and modeling studies. Simulated bow echoes were sensitive to the hail size distribution within the ice microphysics scheme, the coriolis parameter, and surface drag. Future work will involve increasing the horizontal grid resolution and diagnosing mesovortex formation.

Acknowledgements: The research results presented herein were supported by the National Science Foundation under Grant ATM-0233178.

REFERENCES

Atkins, N.T., C.S. Bouchard, R.W. Przybylinski, R.J.Trapp, and G. Schmocker, 2005: Damaging surface wind mechanism within the 10 June 2003 Saint Louis bow echo during BAMEX. *Mon. Wea. Rev.*, **133**, in press.

Fujita, T.T., 1978: Manual of downburst identification for project Nimrod. Satellite and Mesometeorology Research Paper 156, Dept. of Geophysical Sciences, University of Chicago, 104 pp. [NTIS PB-286048]

Trapp, R.J., and M.L. Weisman, 2003: Low-level mesovortices within squall lines and bow echoes. Part II: Their genesis and implications. *Mon. Wea. Rev.*, **131**, 2804-2823.